Revealing the atomic surface structure of the (100) Y-Al-Ni-Co approximant by low-energy electron diffraction and scanning tunneling microscopy

R. Mäder,[1,2] R. Widmer,[1] B. Bauer,[3] P. Gille,[3] P. Gröning,[1] W. Steurer,[2] and O. Gröning[1]
[1]*EMPA, Swiss Federal Laboratories for Materials Testing and Research, nanotech@surfaces Laboratory, Feuerwerkerstrasse 39, CH-3602 Thun, Switzerland*
[2]*Department of Materials, ETH Zurich Laboratory of Crystallography, Wolfgang-Pauli-Str. 10, CH-8093 Zurich, Switzerland*
[3]*Department of Earth and Environmental Sciences, Crystallography Section, Ludwig-Maximilians-Universität München, Theresienstrasse 41, D-80333 München, Germany*

(Received 28 August 2009; revised manuscript received 14 January 2010; published 5 February 2010)

In this paper we present an investigation of the (100) Y-$Al_{75.8}Ni_{2.1}Co_{22.1}$ surface, which is structurally and chemically related to the (10000) twofold symmetric surface of the decagonal Al-Ni-Co quasicrystal. The atomic surface structure was probed by low-energy electron diffraction (LEED) and by scanning tunneling microscopy (STM), revealing three different surface terminations and three different types of surface reconstructions. All three terminations were successfully assigned to the densest bulk layers and the origin of the surface reconstructions revealed by LEED could be identified locally by STM. The (100) Y-Al-Ni-Co surface shares with the related (10000) d-AlNiCo quasicrystal surface the strong tendency of reconstruction, which in the former case is occurring along the *b* axis and in the later along the periodic [00001] direction. Gaining a theoretical understanding of the reconstructions of the (100) Y-Al-Ni-Co surface might therefore help to understand the stability of bulk and surface atomic structures in decagonal quasicrystals. Furthermore, due to the strong relation to the quasicrystalline (10000) d-AlNiCo surface, the crystalline (100) Y-$Al_{75.8}Ni_{2.1}Co_{22.1}$ surface is now a very promising candidate to study directional anisotropies in epitaxial thin film growth, friction, or the electronic structure, with the advantage of representing a much simpler structure (32 atoms/unit cell) which can be theoretically addressed with less effort compared to its quasicrystalline counter part.

DOI: 10.1103/PhysRevB.81.064201 PACS number(s): 61.44.Br, 68.35.B−, 68.37.Ef

I. INTRODUCTION

The discovery of quasicrystals[1] has led to an extensive study relating to the lack of the translational symmetry and its effect on the physical properties of quasicrystalline solids. In this respect the properties of decagonal quasicrystals (d-QC), which can be viewed geometrically as a periodic stacking of aperiodic planes,[2] are particularly interesting. They exhibit a strong anisotropy between the periodic and the aperiodic crystal directions with regard to the friction coefficient[3] as well as the electrical- and thermal-transport properties.[4–7] The question[6] raised here is, whether the anisotropy is related to the long-range aperiodic order of the quasicrystal or to the complex local atomic order on the scale of a few nearest-neighbor distances with no direct relationship to quasicrystallinity. A good way to approach this question is to compare d-QCs with approximants, their periodic counterpart, which present locally similar atomic arrangements but possess a periodic structure. One such analog to the d-Al-Ni-Co quasicrystal is the monoclinic Y-Al-Ni-Co approximant.[8] Both materials exhibit highly anisotropic electrical and thermal conductivities.[6,7,9] This asymmetry, which can amount to a factor of 3–8, is observed between the periodic [00001] direction and the quasiperiodic [10000] direction for the d-Al-Ni-Co and between the *b* axis and the monoclinic direction for the Y-Al-Ni-Co. Smontara *et al.*[7] interpreted these findings such that the long-range quasiperiodicity of the structure is of marginal importance for the anisotropy (if of any importance at all) and attributed it to the complex local atomic order on the scale of nearest-neighbor atoms.

In addition to the anisotropy of bulk properties also the surface can exhibit anisotropic properties, e.g., in the friction coefficient. Furthermore, in the material class of complex metallic alloys, to which the Y-Al-Ni-Co can be attributed, the identification of a particular surface termination can yield information on the stability and energetics of the bulk structure perpendicular to the surface, e.g., by identifying a given surface termination with a particularly stable layer in the bulk structure. On the other hand surface reconstructions (or their absence) lead to information on the in-plane stability.[6,10] Therefore a detailed knowledge of the surface structure is essential. In the case of the (12100) and the (10000) twofold quasicrystal surfaces, scanning tunneling microscopy (STM) studies[3,11–13] reveal a strong tendency to develop an anisotropic surface structure. The (10000) d-Al-Ni-Co surfaces present a columnar structure along the periodic [00001] direction with a well-defined 0.8-nm periodic reconstruction. This reconstruction is also present in the bulk of all d-Al-Ni-Co modifications. Only the basic Ni-rich phase possesses a 0.4-nm periodicity.[14]

The (100) planes of the Y-Al-Ni-Co bulk structure are strongly related to the (10000) planes of the d-Al-Ni-Co bulk structure. The planes of both materials possess a similar atomic structure with a twofold rotational symmetry and a 0.2-nm interplane distance along the axis which lies perpendicular to the aperiodic or monoclinic plane. With the recent advances in the growth of large single-crystal samples, it is now possible to investigate the (100) Y-$Al_{75.8}Ni_{2.1}Co_{22.1}$ surface by high-resolution STM and by LEED. We can conclude that the observed surface structure reveals, similar to the (10000) d-Al-Ni-Co, the expected columnar structure

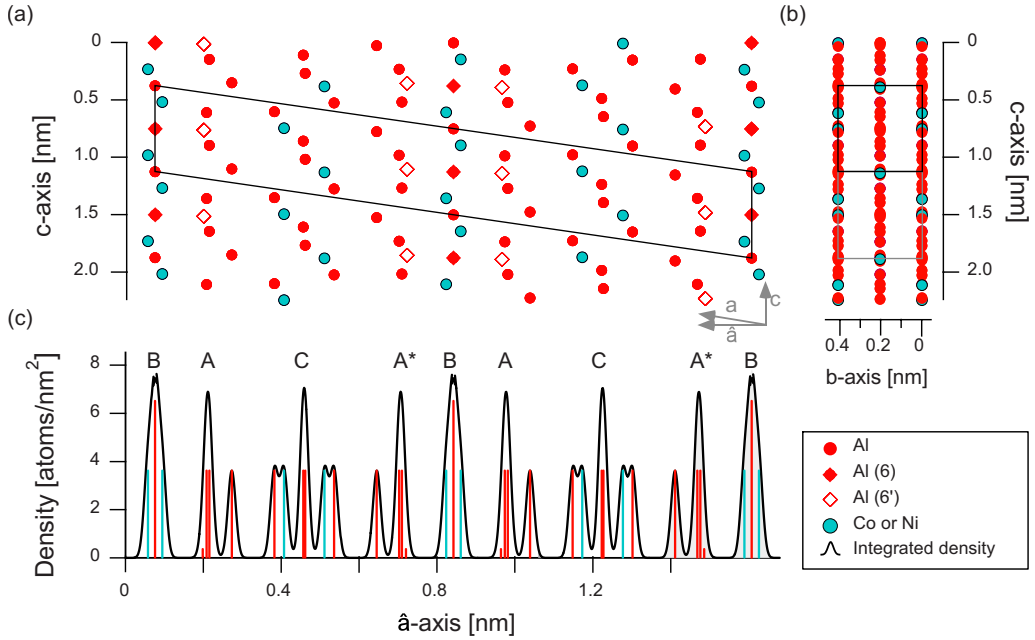

FIG. 1. (Color online) Bulk structure model of Y-Al-Ni-Co (Ref. 8), please note: the axis are differently scaled. (a) The bulk model along the (010) direction with an indicated unit cell (black parallelogram). The Al and Co or Ni atoms are labeled with dark (red) and with bright (turquoise) circles whereas the partially occupied Al(6) 90 % and Al(6′) 10 % atoms are denoted by filled and empty dark (red) squares. (b) The bulk model is shown along the (100) direction with indicated top and bottom view of the unit cell black and gray rectangles. (c) Presents the surface density (atoms/nm^2) of atomic planes perpendicular to the $\hat{a}$ axis. The vertical bars denoting the density are colored according to their composition, dark (red) for 100 % Al and bright (turquoise) for 100 % TM (Co or Ni). The black envelope curve models the integrated density along the $\hat{a}$ axis. Identical highly dense layers are indicated by the same letter A, A*, B, or C.

which can be described as a reconstruction of the densest layers of the bulk model.

II. EXPERIMENTAL DETAILS

The monoclinic Y-$Al_{75.8}Ni_{2.1}Co_{22.1}$ crystal used in this study was grown by using the Czochralski method. The crystal was aligned by means of Laue diffraction and the cut-out (100) surface has been polished to mirrorlike finish by using diamond paste down to a grain size of 0.1 μm. The specified chemical composition of the crystal was further determined by electron probe microanalysis. The following UHV preparation (base pressure below 10^{-10} mbar) was carried out by repeated sputter-annealing cycles. The cycles consisted of Ar^+-ion bombardment at 1 kV and grazing angle of 30° for 30 min followed by 1 h annealing to 1083 K, monitored by an optical pyrometer Raytek MA2B with the emissivity set to $\varepsilon=0.35$. This procedure was repeated six to eight times. The prepared surfaces showed sharp LEED patterns from 15 to 200 eV kinetic electron energy. The subsequent STM measurements were carried out using a commercial UHV Omicron low-temperature STM cooled down with liquid nitrogen (at 77 K) or liquid helium (at 5 K). Scanning at cryogenic temperature reduces thermal drifts and the cold cryostat enhances the local pressure which allows us to measure over several days the same clean surface. During the measurements no temperature dependency of the surface structure is observed. Mechanically cut Pt_{80}/Ir_{20} tips were used for the STM imaging and the recorded STM data was further processed by the WSXM software.[15]

III. RESULTS AND DISCUSSION

The (100) Y-Al-Ni-Co surface structure is considered[8] as a crystalline counterpart to the low-index (10000) twofold d-Al-Ni-Co surface. We based our analysis of the surface structure on the structure solution of the $Al_{13-x}(Ni_yCo_{1-y})_4$ compound of Zhang *et al.*[8] and will also use their notation for crystal directions and planes. The bulk structure of the Y-Al-Ni-Co is found to be identical[16] to the $Al_{13-x}(Ni_yCo_{1-y})_4$ structure (with $x=0.9$ and $y=0.12$) which is one representative of the $Al_{13}TM_4$ class of decagonal approximants. The unit cell of the $Al_{13-x}(Ni_yCo_{1-y})_4$ structure contains 32 atoms (24 Al and eight Co or Ni) and has the lattice parameters [space group $C2/m$ (No.12)] $a=17.071(2)$ Å, $b=4.0993(6)$ Å, $c=7.4910(9)$ Å, and $\beta=116.17(1)°$. The 32 atoms per unit cell are placed on nine crystallographically inequivalent sites (seven Al and two Co or Ni sites). Two of the nine Al sites are partially occupied [Al(6) 90% occupancy and Al(6′) 10% occupancy]. Along the b axis, the [010] direction, the Y-Al-Ni-Co crystal structure consists of a 0.41-nm periodic stacking of two atomic planes of the same type. These two planes are related to each other by a 2_1 screw axis and separated by 0.205 nm. The $Al_{13-x}(Ni_yCo_{1-y})_4$ bulk structure and the introduced nomenclature of Zhang *et al.*[8] is illustrated in Fig. 1. The bulk

structure model oriented along the [010] axis is shown in Fig. 1(a) where the atomic sites are marked by bright full circles (turquoise) for Co or Ni and by dark (red) full circles for Al atoms. The partially occupied Al(6) 90% and Al(6′) 10% sites are labeled by dark (red) full squares and dark (red) empty squares. Figure 1(b) shows the (100) plane of the bulk model which represents the view onto the investigated surface. Figure 1(c) displays the surface density of planes along the $\hat{a}$ axis. Please note that the $\hat{a}$ axis is tilted with respect to the a axis by 26.17° and therefore lies parallel to the (100) surface normal. The surface density (vertical lines) in Fig. 1(c) denotes the number of atoms per nm^2 having the same position with respect to the $\hat{a}$ axis taking into account the partial occupancy. To emphasize possible surface terminations adjacent planes are grouped together. This grouping is performed by superimposing a narrow Gaussian for each plane which is weighted by the calculated density. The set of Gaussians is then added up, resulting in the density modulation chart which is indicated by the black line. The density profile shows that four inequivalent highly dense, well-separated, combined planes are present (which will be referred to as layers from now on). The corresponding chemical composition is indicated by color whereas 100% Al (dark, in color version red) or 100% TM (Co or Ni, bright, in color version turquoise) layers are present. These layers are labeled in Fig. 1(c) by the letters A, A*, B, and C. The pure aluminum A and A* layers are related to each other by a twofold rotational axis which stands perpendicular to the (010) plane. The A and A* layers consists of Al(2), Al(7), or the partially occupied Al(6′) (10%) sites, respectively. The density of the A layers is around 6.9 atoms/nm^2. On the other hand the B layer possessing the highest density of 7.8 atoms/nm^2 is composed of three planes: the central plane consisting of Al(1) and partially occupied (90%) Al(6) sites and two pure TM planes on either side of the central Al one. An enlarged representation of the sequence of the atomic sites of the A and B layers is shown in Fig. 4(b). The last of the high-density layers, the C layer with a density of 7.0 atoms/nm^2, is composed of two Al planes which consist of the Al(3) sites. This C layer is flanked by two less dense layers which consist of a Al(5) and TM plane.

Figures 2(c) and 2(d) show representative three-dimensional STM images of stepped (100) Y-Al-Ni-Co surface areas. The (100) Y-Al-Ni-Co surface shows well-defined atomically flat terraces separated by steps of different heights. The terrace step heights are illustrated in Fig. 2(b) by taking a short and a long line profile along the shown path in the Figs. 2(c) and 2(d), respectively. The line profile of Fig. 2(c) represents a step height sequence within one bulk unit cell, whereas the profile of Fig. 2(d) extends over more than one bulk unit cell. The dashed lines in Fig. 2(b) indicate the step height sequence of the measured terraces. By comparing Fig. 2(a) [analog to Fig. 1(c) while reading from top to bottom] with Fig. 2(b) a very strong correlation between the measured step height sequences and the density profile of the high density A, B, and C bulk planes[8] is obvious. Taking a closer look we see that the short profile already shows a sequence which contains all three layer types. Over an extended height range (4.5 nm) the measured step heights follow perfectly the sequence of the high-density bulk layers as

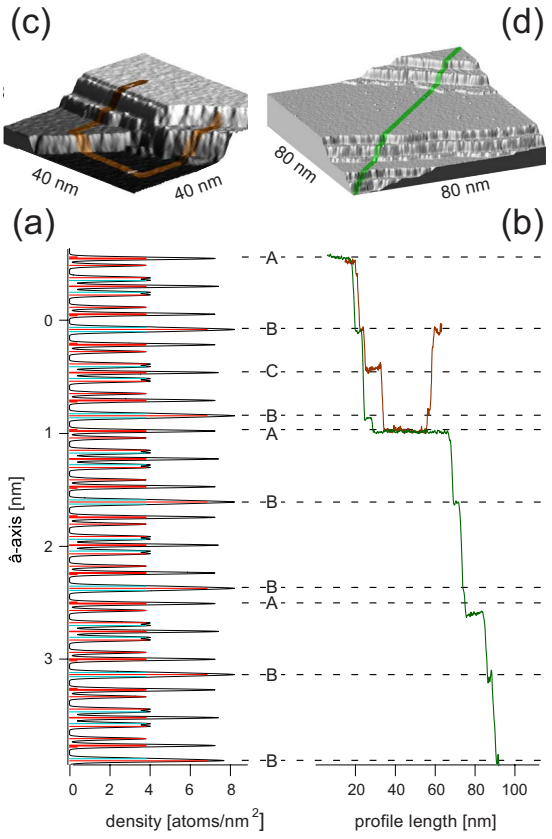

FIG. 2. (Color online) Step heights analysis of the (100) Y-Al-Ni-Co surface. (a) Shows the density (atoms/nm^2) of the bulk layer versus the $\hat{a}$ axis. (b) Two STM image profiles bright and dark (brown and green) taken along terraced (100) surface areas. The corresponding profile paths are overlaid on the three-dimensional STM images presentations in (c) recorded at V_T=−0.5 V and I_T =0.169 nA, T=77 K for the brown and (d) recorded at V_T= −0.75 V and I_T=1 nA, T=77 K for the green path.

well. The absolute values of the step heights can be obtained by considering that the shortest distance between B layers is $\frac{1}{2}$ of the $\hat{a}$-axis lattice vector of 15.25 Å, the distance between C and B layers is $\frac{1}{4}$ of the $\hat{a}$ axis and the distance between the B and A layers is 1.34 Å. In addition we could identify by STM for each type of termination A, B, and C a distinctive surface structure. However, the frequency of occurrence of the three terminations is not equally distributed. The most commonly observed termination layer is the A followed by the B type and the rarely occurring C-type layer. An interesting point to notice is that after investigating many step height sequences only the A-layer type is present whereas of the A*-layer termination is absent. This means that the surface induces a preferential direction along the $\hat{a}$ axis (going from vacuum to bulk) which influences the termination stability. The conclusion from the absence of the A*-layer termination is that the underlying layer(s) play evidently an important role in the surface stability. Indeed the situation is different for an A* layer which is followed into the bulk by the dense B layer whereas the A layer has only one but well-separated single Al layer directly underneath.

The interesting question now is whether these three terminations possess surface structures which correspond to the

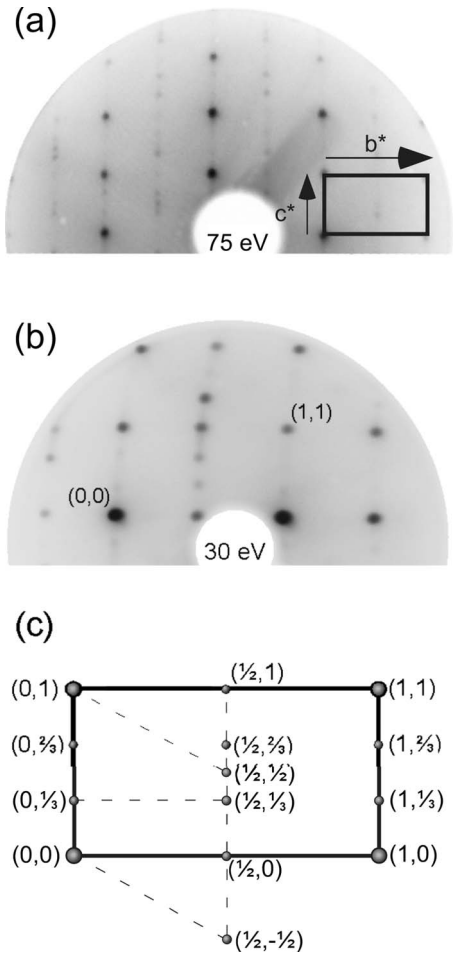

FIG. 3. LEED analysis of the (100) Y-Al-Ni-Co surface (inverted gray scale for clarity). (a) Presents the LEED pattern recorded at 75 eV. In the lower part a magnification of (a) of only one unit cell is shown. (b) For a detailed spot analysis a pattern recorded at 30 eV of a slightly tilted surface is shown. (c) A sketch labeling the observed diffraction spots in the unit cell (solid black rectangle) is given. The unit cell of the reconstructions are indicated by dashed squares.

ones of the truncated bulk at the corresponding layer positions. Therefore we performed a qualitative LEED analysis of the (100) Y-Al-Ni-Co surface. Two representative LEED patterns recorded at 75 eV [Fig. 3(a)] and at 30 eV [Fig. 3(b)] are presented. Both patterns show sharp and intense (1×1) spots of the (100) Y-Al-Ni-Co surface reciprocal unit cell which is labeled in Fig. 3(a). Furthermore, a number of faint spots are visible. To label these spots a sketch containing all diffraction spots, observed with different intensities at different energies, within the reciprocal unit cell is given in Fig. 3(c). At lower electron energy (30 eV) the LEED pattern in Fig. 3(b) shows a magnified pattern with the surface tilted so that the specular spot is off-centered as indicated. The major deviation to the 70 eV LEED pattern is the enhancement of the (1/2,0) and (1/2,1) spots and the attenuation of the (1/2,1/2) spot.

The observed LEED patterns are interpreted with the aid of subsequently recorded STM images (and discussed below). In Fig. 3(c) a sketch of the reciprocal (100) surface unit cell is indicated by full lines whereas by dashed lines the unit cells of the reconstructions are outlined. We identified three incoherently superimposed surface reconstructions: a (2×1) reconstruction which leads to the (1/2,0) and (1/2,1) diffraction spots, a (2×3) reconstruction which gives rise to the (0,1/3), (1/2,1/3), (1,1/3) and the (0,2/3), (1/2,2/3), (1,2/3) spots, and a $c(2\times2)$ reconstruction which produces the (1/2,1/2) spot.

We are now confronted with the situation of having three different terminations and three different reconstructions. Therefore, the challenge is to describe and address these three reconstructions to the three identified terminations on an atomic scale by STM. We start this discussion with the most frequently observed termination, the A termination which is shown in Fig. 4(a). In this representation the *c* axis lies horizontally and the 0.4-nm periodic *b* axis vertically. The surface structure reveals a strong columnar atomic arrangement along the *c* axis. These columns are clearly defined and show the bulk periodicity of 0.4 nm along the *b* axis. Between two columns we observe adatomlike features, indicated by a red arrow, which double the periodicity to 0.8 nm along the *b* axis. These adatoms also create a vertical columnar surface structure. In general, the surface structure presents a (2×1) reconstruction but some remaining features of the unreconstructed (100) bulk unit cell is still visible which is indicated in Fig. 4(a) by the rectangle A. The unit cell of the dominating (2×1) reconstruction is denoted by the rectangle B. The inset in Fig. 4(a) shows the fast Fourier transformation (FFT) of the presented STM image. Spots corresponding to a doubled periodicity of 0.8 nm in the *b*-axis direction can be observed (indicated by a black arrow) which demonstrates clearly that a (2×1) reconstruction is present.

One obvious feature is that the (2×1) reconstruction is not regular. Some unit cells of the reconstruction are shifted along the *b* axis. To visualize these shifts we calculated the cross-correlation map of the STM image with the unit cell of the (2×1) reconstruction. The reference unit cell of the (2×1) reconstruction is indicated by the rectangle R in Fig. 4(a). Figure 4(c) presents the resulting correlation pattern as a contour plot overlaid on the original STM where the intensity is given by color, ranging from low intensity dark (red) to high intensity bright (yellow). The highly intense spots on the pattern show the center of the unit cell of the (2×1) reconstruction. We see that this reconstruction is partitioned into three vertical domains where the middle domain is shifted along the *b* axis by half of the (2×1) superlattice vector with respect to the adjacent domains. The domain boundaries are indicated in Figs. 4(a) and 4(b) by (pink) lines. Moreover, the presence of the two shifted (2×1) domains proves again that we are indeed confronted with a surface reconstruction.

Since we have successfully identified the corresponding bulk layer of the A termination by the analysis of step heights, a structural comparison can be performed. An atomic structure representation of the (100) A layer from the bulk structure is shown in the upper right inset of Fig. 4(b). The atom sites are labeled by (red) full circles Al(2), full (red) squares Al(7), and empty (blue) squares for the partially occupied Al(6′) according to the corresponding bulk layer,

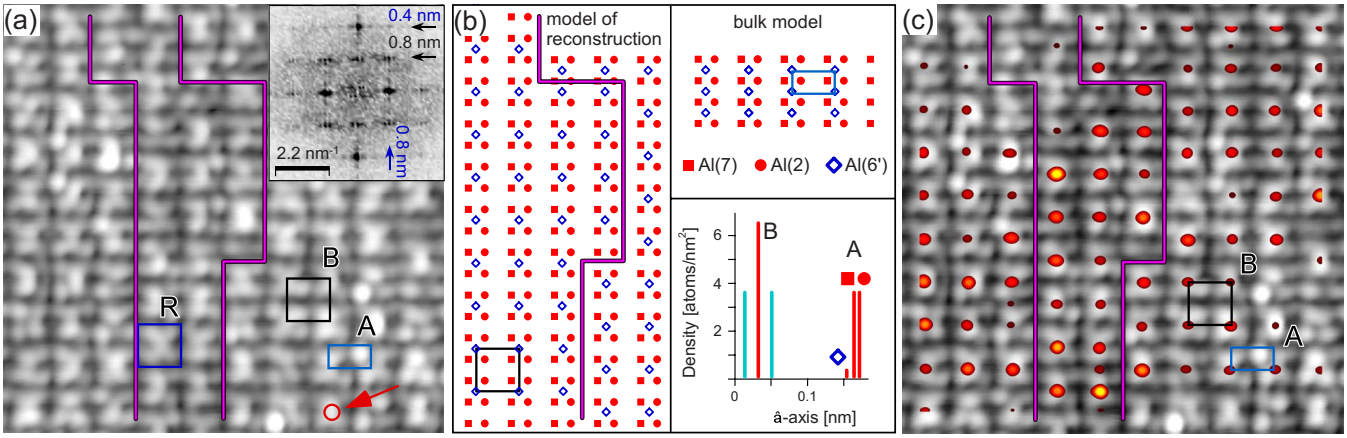

FIG. 4. (Color online) Structure analysis of the A termination. (a) 8×7.8 nm^2 STM image recorded at $V_T=+0.05$ V, $I_T=0.234$ nA, and $T=77$ K. On the lower right the unit cell (rectangle A) and the unit cell of the (2×1) reconstruction (rectangle B) are indicated. The borders of the phase shift between the unit cells of the (2×1) reconstruction are indicated by (pink) lines. The inset shows the FFT of the STM image. (b) same scale as (a), top-right panel: the A layer of the bulk model with a 100% occupancy of the Al(6′) sites is presented; the lower-right panel shows the atom labeling in the density versus $\hat{a}$-axis chart. The left part visualizes the A layer of the bulk model with a 50% occupation of the Al(6′) sites, the unit cell of the (2×1) reconstruction is indicated. (c) Presents the same STM image as in (a) superimposed by the cross-correlation pattern of the unit cell of the (2×1) reconstruction [rectangle B in (a)] with the STM image (see text).

as indicated in the inset on the lower right-hand side. As mentioned above the view direction along the surface normal ($\hat{a}$ axis) is from B to A layers (e.g., left to right in Fig. 1). Therefore, the plane of the partially (10%) occupied Al(6′) sites lies on top of the other two planes composed of Al(7) and Al(2) sites. The depicted A layer of the bulk structure in the upper part of Fig. 4(b) can be regarded as a regular grid of Al(7) and Al(2) sites on top of which all possible sites of the Al(6′) atoms are indicated by (blue) empty squares. The analogy to the presented STM image in Fig. 4(a) is now apparent: the Al(7) and Al(2) sites are forming the horizontally laying columns along the c axis and the Al(6′) atoms, which we might regard as adatoms, are situated between these columns. In the inset on the left-hand side of Fig. 4(b) we modeled a 50% occupation of the Al(6′) sites. In this model we also performed a vertical shift of a half of the (2×1) superlattice vector between the Al(6′) sites. The domain boundary is again indicated by a (pink) line. The resulting picture closely resembles the measured STM image of the A layer. The comparison between the A layer of the bulk model and the measured A termination shows that around 50% of the Al(6′) sites are occupied instead of the 10% originate from the bulk model. It is quite reasonable that the occupation density for the Al(6′) sites is higher than predicted by the bulk model since on the surface the restriction of the occupation by overlaying layers is not present. The higher occupation frequency of the Al(6′) sites can be explained by atom surface diffusion due to the sputtering and annealing procedure used for the preparation. This proposed 50% occupation density model for the Al(6′) at the surface is consistent with reasonable interatomic distances (~0.26 nm not considering surface relaxation) and density of the A layer (8.6 atoms/nm^2). A second deviation from the bulk structure model is that the surface corrugation revealed a bimodal height distribution with a separation of the two components of 0.27 Å, which is around 0.1 Å larger than the interbulk layer separation of the A termination of the bulk model structure. This difference might originate from electronic effects or is due to a surface relaxation.

In addition to the presented high-resolution STM image analysis of the A termination we performed a series of STM measurements recorded at the same location (7.4×7.4 nm^2) but at different sample biases to give a first indication of the density of states (DOS) distribution of the electrons at the surface. The bias dependency analysis of the A termination is presented in Fig. 5 where the same spot in each image is indicated by a (red) cross. Starting the series from −1 V Fig. 5(a) we observe a strong anisotropy in form of vertical stripes along the b axis. Decreasing the sample bias down to −0.5 V and further down to −0.3 V the vertical stripes are more and more shaped as chains. Two unit cells are indicated in Fig. 5(c). At positive sample bias, presenting the unoccupied states, starting at +0.3 V the A termination shows more of a striped image oriented along the horizontally laying c axis. This appearance changes drastically when increasing the sample bias slightly to +0.5 V. Stripes oriented along the b-axis turn up while at +1 V the surface structure shows a contorted tubelike appearance. Ex-

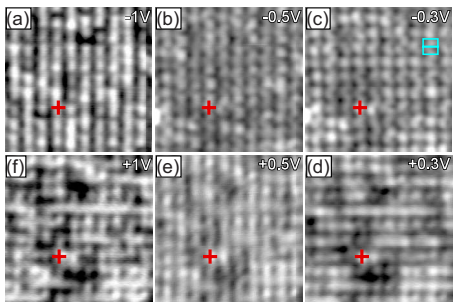

FIG. 5. (Color online) Bias dependency of the A termination. Series of STM images (7.4×7.4 nm^2, $I_T=1$ nA, and $T=5$ K) recorded at the same location which is indicated by a red cross. The sample bias is indicated on the upper right. In (c) two unit cells are drawn in on the upper part of the image.

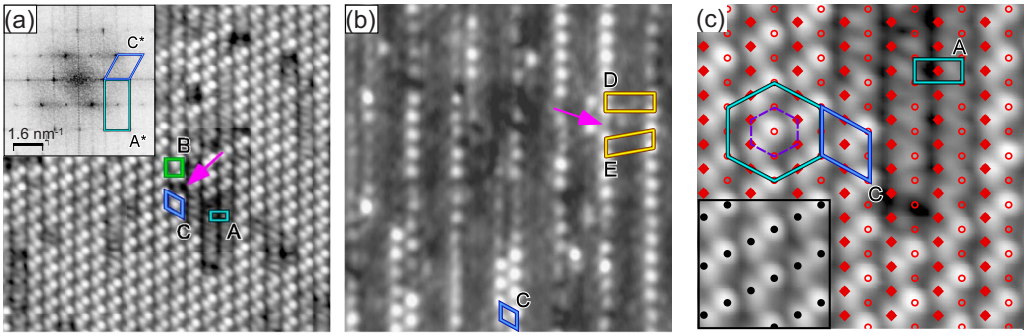

FIG. 6. (Color online) Surface-structure analysis of the B termination. (a) 15×15 nm^2 STM image recorded at +0.3 V sample bias, I_T=0.15 nA and T=77 K. The measured B termination consists of two layers separated by around 0.4 Å. The upper layer shows the $c(2\times2)$ reconstruction denoted by the parallelogram C (blue) and the rarely observed (2×1) reconstruction indicated by rectangle B (green). The position of the phase shift between those two reconstructions is pointed out by the arrow. On the lower layer the undistorted bulk model unit cell is indicated by the rectangle A. The inset shows the FFT of the STM image. (b) STM image of a less dens upper layer of the B termination, same scan condition as (a). The developed vertical rows along the *b* axis creates different reconstructions: the $c(2\times2)$ reconstruction indicated by the parallelogram C (blue), a (2×3) reconstruction labeled by rectangle D (yellow) and a $(2\times3.04)-10.33°$ reconstruction outlined by the parallelogram E (yellow). (c) 5×5 nm^2 zoom in of the STM image presented in (a). Bulk atom positions are overlaid, where Al(1) and Al(6) are indicated by (red) squares and by (red) circles, respectively. On the upper right the bulk model unit cell is indicated and on the upper left the hexagonal structure of the B termination and the inflated reconstruction is shown. The lower-left inset presents a perfect match of selected bulk atom sites (full black circles) with the measured surface structure.

plaining the changes in the surface appearance by varying the applied sample bias would require an in-depth density-functional-theory calculation, thus it is beyond the scope of this work. Nevertheless, this series shows the distribution of the DOS of the electrons at the surface. The DOS is strongly energy dependent and not symmetrical distributed at the surface with respect to the Fermi level since for the same applied sample bias value the occupied and unoccupied states appearance is clearly different. A strong tendency to develop anisotropic surface structures is observed. This might be an experimental indication on atomic scale to explain the observed anisotropic electronic transport in literature.[4–6]

We turn now to the discussion of the second most frequently observed termination, the B termination. The STM image in Fig. 6(a) shows a 15×15 nm^2 section of the B termination. Similarly to the A also the B termination presents a columnar surface structure along the *b* axis. The surface structure shows clearly a two-layer structure by analyzing the measured height distribution. It reveals a bimodal height distribution with a separation of the two components by 0.42 Å. The lower lying layer presents the bulk structure periodicity which is indicated by rectangle A. This part of the surface structure appears as vertical stripes along the *b* axis with a zigzag pattern. Directly above the zigzag stripes in the upper layer we observe vertical stripes of circles in couples. The structure of the upper layer, such as the A termination, has a doubled bulk structure periodicity along the *b* axis. This reconstruction is indicated by the parallelogram C in Fig. 6(a) and is identified to be the $c(2\times2)$ one which we already came across during the analysis of the LEED patterns. Equivalent to the A termination we notice on the B termination that the reconstruction can be distorted by a shift of half of the superlattice vector along the *b* axis. This results in a local (2×1) unit cell which is indicated by the rectangle B and the location of the shift is pointed out by the (pink) arrow. This shift of one half of the superlattice vector along the *b* axis in the upper layer emphasizes that the underlying layer possesses the bulk structure periodicity of 0.4 nm. The inset in Fig. 6(a) shows the FFT of the presented STM image where the bulk unit cell labeled as A* as well the $c(2\times2)$ reconstruction labeled as C* are indicated. The most dominating FFT spots derive from the $c(2\times2)$ reconstruction which lead to the distorted appearing of the FFT image and the development of the (1/2, 1/2) spot as mentioned in the LEED discussion.

Less frequently but with the same step height sequence we observed a B termination with a decreased density in the upper layer. In Fig. 6(b) a 15×15 nm^2 section of such a B termination is presented. The STM image shows vertical chains with a doubled bulk structure periodicity along the vertical *b* axis. The same $c(2\times2)$ reconstruction as in Fig. 6(a) is observed when two vertical chains are directly in contact with each other, indicated by the parallelogram C. Additionally we can identify, at this low-density upper layer, the last of the three reconstruction observed by LEED. This (2×3) reconstruction is shown in Fig. 6(b) by the rectangle D (yellow), in areas where the vertical chains are well separated from each other. The yellow arrow indicates a shift of half the superlattice vector in the *b*-axis direction, which, as in the other cases, underlines the nature of this structure being a reconstruction.

Now we turn to a description of the B-layer structure and the identification of atomic sites in the STM topography. In Fig. 6(c) we present a 5×5 nm^2 zoom of Fig. 6(a) which is overlaid with the atomic positions of the pure aluminum layer consisting of Al(1) and the partially occupied (90%) Al(6) sites which are indicated by (red) squares and by (red) circles, respectively. The sum of both Al sites creates a hexagonal pattern which is indicated by dashed (purple) lines. With this pattern the upper layer surface structure of the B termination cannot be described, but considering the next larger hexagon, indicated by full (turquoise) lines, the verti-

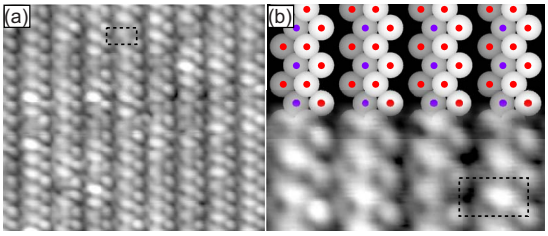

FIG. 7. (Color online) Surface-structure analysis of the C termination. (a) 6.5×5.6 nm^2 STM image recorded at $V_T=+0.1$ V sample bias, $I_T=0.2$ nA and $T=77$ K. The C termination shows the bulk periodicities, the unit cell is indicated in the upper part by a dashed rectangle. (b) Comparison study of the measured surface (lower part) with the C layer of the bulk model (upper part). The structure model is illustrated by circles with a centered colored spot, red for aluminum and blue for the transition metals, Co or Ni. The unit cell is again denoted by a dashed rectangle.

ces of the $c(2\times2)$ unit cell (parallelogram C) are reached by the vertices of the large hexagon. To fully describe the observed B termination we see that every second diagonal Al row must vanish. We illustrate in the inset on the lower left of Fig. 6(c) such a selection of Al sites from the bulk structure model overlaid on the STM image where a perfect match with the experiment is achieved. On the other hand the surface structure analysis of the lower layer of the B termination is not that straightforward. Neither the dense Al layer consisting of Al(1) and Al(6) sites nor the adjacent Co layers show such a ribbon with a zigzag structure along the *b* axis.

Continuing the description of the terminations along their frequency of appearance, we focus now on the least frequently observed C termination. The observed surface structure is presented in Fig. 7(a) by a 6.5×5.6 nm^2 STM image. It again shows a columnar structure along the *b* axis with a clear 0.4-nm bulk periodicity. To illustrate the relation with the bulk structure we marked the (1×1) bulk unit cell by dashed lines in the upper part of the STM image. The lower part of Fig. 7(b) represents a zoom-in of Fig. 7(a) where the surface structure details of the C termination are now more apparent. We see four columns along the *b* axis where each of the columns is adjacent on the right by a chain of supposedly single atoms. The bulk unit cell is again indicated by a dashed rectangle. To relate the measured surface structure with the bulk atomic sites we show in the upper part of Fig. 7(b) the selected layers of the bulk structure. It turned out that the density (atoms/nm^2) of the C layer is too low to mimic the surface structure. Therefore, also the underlying layers must be taken into account. Since we know that the view direction is from C to A*, along the surface normal ($\hat{a}$ axis) in the bulk structure model we can conclude that below the C termination is a TM layer, and further below a Al(5) layer is present [consider Fig. 1(c)]. The height difference between these three bulk layers in Fig. 7(b) is indicated by the gray scale of the white circles where the color in the center of the circles labels the atom type, red for Al and blue for TM. The bright white surrounded Al sites and is therefore the top layer which consists of Al(3) sites. This Al(3) layer represents the already mentioned additional chain on the right-hand side of the columnar structure. The TM layer (blue) and the lower Al(5) layer form the body of the columns. In general these three layers simulate quite well the STM image of Fig. 7(b) by showing the four columns with the appropriate dimensions.

IV. CONCLUSION

We have investigated the (100) surface structure of the monoclinic Y-$Al_{75.8}Ni_{2.1}Co_{22.1}$ crystal by LEED and STM. The study revealed three (labeled here as A, B, and C) atomically flat but structurally inequivalent terraces. The step height sequence of the terraces corresponds well with the sequence of the densest bulk layers. This is in line with termination layers in other complex metallic alloys[17–19] and quasicrystals.[11,20–22] Moreover, the surface structure of all three terminations could successfully be obtained by only slight modifications to the appropriate bulk layers. The modifications were necessary because the A and B terminations present three different surface reconstructions. It could be shown that the two partially occupied Al sites are strongly involved in the surface reconstructions and adopt occupancies at the surface which differ from the ones in the bulk. The common feature of the three surface reconstruction types is the doubling of the bulk periodicity along the *b* axis from 0.4 to 0.8 nm. In addition, all three terminations of the (100) Y-Al-Ni-Co surface show a clearly anisotropic surface structure in the form of columns oriented along the *b* axis. A similar behavior is observed on the related quasicrystalline d-Al-Ni-Co (10000) surface, where two different terminations are found, which possess a clear columnar structure along the periodic direction with a periodicity twice as large as the 0.4-nm dominant stacking sequence of the bulk structure model. Furthermore, the bias-dependent STM imaging of the A-type (100) Y-Al-Ni-Co termination shows energy-dependent stripe features in the *b* and *c* directions. This might be an experimental indication on atomic scale to explain the observed anisotropic transport effects.[4–7] In our ongoing studies of the surface electronic properties of the d-Al-Ni-Co and Y-Al-Ni-Co we will be investigating this feature in more detail.

Our study and characterization of the (100) Y-Al-Ni-Co surface should serve as a basis for theoretical modeling of the energetics of the different surface terminations and reconstructions. Such theoretical modeling might help to understand what types of atomic structures are responsible for the formation of stable surface terminations in complex metallic alloys and related quasicrystals. This understanding in turn would allow gaining a deeper understanding of the stabilization mechanisms in the bulk of these materials.

ACKNOWLEDGMENTS

The Swiss National Foundation (Contract No. SNF 200021-112333/1), the European Network of Excellence (NoE): "Complex Metallic Alloys" CMA (Contract No.: NoE 500140), and the EU-FP7: "appliCMA" project (Grant agreement No.: NMP3-SL-2008-214407) are acknowledged.

[1] D. Shechtman, I. Blech, D. Gratias, and J. W. Cahn, Phys. Rev. Lett. **53**, 1951 (1984).
[2] W. Steurer, T. Haibach, B. Zhang, S. Kek, and R. Luck, Acta Crystallogr., Sect. B: Struct. Sci. **49**, 661 (1993).
[3] J. Y. Park, D. F. Ogletree, M. Salmeron, R. A. Ribeiro, P. C. Canfield, C. J. Jenks, and P. A. Thiel, Science **309**, 1354 (2005).
[4] M. Komelj, J. Ivkov, A. Smontara, P. Gille, P. Jeglic, and J. Dolinsek, Solid State Commun. **149**, 515 (2009).
[5] J. Dolinsek, A. Smontara, O. S. Barisic, and P. Gille, Z. Kristallogr. **224**, 64 (2009).
[6] A. Smontara, I. Smiljanić, J. Ivkov, D. Stanić, O. S. Barišić, Z. Jagličić, P. Gille, M. Komelj, P. Jeglič, M. Bobnar, and J. Dolinšek, Phys. Rev. B **78**, 104204 (2008).
[7] A. Smontara, D. Stanic, I. Smiljanic, J. Dolinsek, and P. Gille, Z. Kristallogr. **224**, 56 (2009).
[8] B. Zhang, V. Gramlich, and W. Steurer, Z. Kristallogr. **210**, 498 (1995).
[9] S. Martin, A. F. Hebard, A. R. Kortan, and F. A. Thiel, Phys. Rev. Lett. **67**, 719 (1991).
[10] A. Nduwimana, X. G. Gong, and X. Q. Wang, Appl. Surf. Sci. **219**, 129 (2003).
[11] J. Y. Park, D. F. Ogletree, M. Salmeron, R. A. Ribeiro, P. C. Canfield, C. J. Jenks, and P. A. Thiel, Phys. Rev. B **72**, 220201(R) (2005).
[12] J. Y. Park and P. A. Thiel, J. Phys.: Condens. Matter **20**, 314012 (2008).
[13] M. Kishida, Y. Kamimura, R. Tamura, K. Edagawa, S. Takeuchi, T. Sato, Y. Yokoyama, J. Q. Guo, and A. P. Tsai, Phys. Rev. B **65**, 094208 (2002).
[14] S. Katrych and W. Steurer, Z. Kristallogr. **219**, 606 (2004).
[15] I. Horcas, R. Fernandez, J. M. Gomez-Rodriguez, J. Colchero, J. Gomez-Herrero, and A. M. Baro, Rev. Sci. Instrum. **78**, 013705 (2007).
[16] S. Kek, Ph.D. thesis, University of Stuttgart, 1991.
[17] H. R. Sharma, M. Shimoda, V. Fournee, A. R. Ross, T. A. Lograsso, and A. P. Tsai, Phys. Rev. B **71**, 224201 (2005).
[18] J. Smerdon, J. Parle, R. McGrath, B. Bauer, and P. Gille, Z. Kristallogr. **224**, 13 (2009).
[19] R. Addou, E. Gaudry, T. Deniozou, M. Heggen, M. Feuerbacher, P. Gille, Y. Grin, R. Widmer, O. Groning, V. Fournee, J. M. Dubois, and J. Ledieu, Phys. Rev. B **80**, 014203 (2009).
[20] N. Ferralis, K. Pussi, E. J. Cox, M. Gierer, J. Ledieu, I. R. Fisher, C. J. Jenks, M. Lindroos, R. McGrath, and R. D. Diehl, Phys. Rev. B **69**, 153404 (2004).
[21] J. Ledieu, E. J. Cox, R. McGrath, N. V. Richardson, Q. Chen, V. Fournee, T. A. Lograsso, A. R. Ross, K. J. Caspersen, B. Unal, J. W. Evans, and P. A. Thiel, Surf. Sci. **583**, 4 (2005).
[22] R. Mäder, R. Widmer, P. Gröning, S. Deloudi, W. Steurer, M. Heggen, P. Schall, M. Feuerbacher, and O. Gröning, Phys. Rev. B **80**, 035433 (2009).